The Bioelectrics of Immortality and Mortality in Cold-Sensitive *Hydra oligactis*

Stefania E. Kapsetaki, PhD,[1] Angelina Pimkina, PhD,[1,2] Patrick McMillen, PhD,[1,3] Parande Tayyebi, PhD,[1] Patrick Erickson, PhD,[1] and Michael Levin, PhD[1,3,4]

Abstract

Introduction: Bioelectric properties of cells are an important aspect of development, regeneration, and cancer. Because of their relevance to the establishment and maintenance of tissue form and function, bioelectric patterns have been hypothesized to have a role in aging. However, no data on bioelectric patterns of the whole body of young and old individuals have been available.

Methods: We observed and quantified the bioelectrics of whole-body immortal (growing at 22°C) and aging mortal (growing at 10°C) cold-sensitive *Hydra oligactis*.

Results: We found that the membrane-voltage-sensitive dyes FluoVolt and VF2.1.Cl can be used to reveal large-scale patterns of cellular membrane resting voltage potentials in hydra. The consensus whole-body bioelectric atlas of immortal hydra shows a consistently depolarized foot and occasionally depolarized tentacles. Immortal hydra are, on average, more depolarized and exhibit less sharply defined bioelectric patterns than old mortal hydra. Immortal hydra have a sharper foot:central body ratio than old mortal hydra.

Conclusions: These data establish hydra as the first model system in which whole-body bioelectric imaging can be performed; the different bioelectric patterns of immortal versus old mortal hydra are consistent with a bioelectric component to the aging process and suggest a roadmap for using this model organism in antiaging therapeutic screens involving electroceuticals.

Keywords: bioelectric map, bioelectric atlas, cnidaria, hydrozoa, bioelectric pattern, membrane voltage, V_{mem}, resting potential

Introduction

Aging presents as a severe, progressive reduction in functional capacity and quality of life with a 100% penetrance.[1,2] It also presents fascinating fundamental questions in evolutionary, cell, and developmental biology with respect to the algorithms implemented by living tissues to maintain form and function against disorder.[3–12] Numerous theories of the underlying molecular causes of aging have been proposed.[13–21] One set of approaches focuses on the progressive degradation of developmental information—cues that allow tissues to maintain a complex morphology for decades while materials and individual cells move in and out of the body. Since one key aspect of this information structure is maintained in bioelectrical gradients of resting potential across tissues,[22–24] it has been suggested that degradation of specifically bioelectric information could be a cause of aging.[25,26]

Patterns of cellular resting potential (V_{mem}) have been measured in a variety of embryonic, regenerative, and oncogenic contexts,[27–31] due to the known role of developmental bioelectricity in regulating morphogenesis and cancer suppression.[22,23] However, no data are currently available on large-scale bioelectric profiles during aging *in vivo* in any model species. This is a rate-limiting step in the development of electroceuticals for longevity. Moreover, additional bioelectricity-relevant approaches involve applying specific electromagnetic fields and pulsed electromagnetic fields to slow down aging,[32–34] performing transcranial direct current stimulation and transcranial magnetic stimulation to improve the declining cognitive functions,[35,36] regulating the body's ion channels with morphoceuticals[25,37] or gero-electroceuticals,[38]

---

[1]Department of Biology, Tufts University, Medford, Massachusetts, USA.
[2]Department of Biomedical Engineering, Tufts University, Medford, Massachusetts, USA.
[3]Allen Discovery Center at Tufts University, Medford, Massachusetts, USA.
[4]Wyss Institute for Biologically Inspired Engineering, Harvard University, Boston, Massachusetts, USA.

bioelectrically controlling stem cells such as their ability to differentiate or continue regenerating,[39] and regulating the restoration of the body's aging bioelectrics with implantable and wearable bioelectronic devices.[40] Evaluating, improving, and extending these pioneering approaches require a better understanding of the bioelectric pattern of young versus old individuals. Thus, we sought to establish a dataset on whole-body bioelectric imaging in a model system that is relevant for aging research.[41–43]

Hydra are relatively small freshwater invertebrates. They have endodermal and ectodermal tissues and can reproduce both sexually and asexually.[44] They have been used as a model organism in many studies[45] focusing on morphogenesis,[46,47] environmental ecotoxicology,[48,49] bacteriology,[50] regeneration,[41,51,52] biomechanics,[53] evolution of multicellularity,[54] morphogenesis and physiology,[55,56] transplantation biology,[45] tumor biology,[57–59] whole-body neural and muscle activity via calcium imaging,[60–63] apoptosis,[43,64] and aging.[42,65]

Their body is transparent, enabling membrane voltage (V_{mem})-sensitive dyes[66–68] to easily penetrate and reveal cellular membrane voltage of the whole organism. At 22°C, cold-sensitive (CS) *Hydra oligactis* are immortal. However, at 10°C, CS *H. oligactis* begin to switch to sexual reproduction and produce ovaries and testes within 3–4 weeks.[69,70] Within 30 days at 10°, CS *H. oligactis* undergo aging[71] and eventually die by day 150.[71] It is known that 80% of the human aging genes from the Human Ageing Genomic Resources (http://genomics.senescence.info) are conserved in hydra.[42] Aging CS *H. oligactis* are less able to grab prey, perform spontaneous contractions, transfer food to their gut, and have fewer sperm and nurse cells after 2 months, fewer numbers of interstitial stem cells, and fewer epithelial cells.[71] This makes CS *H. oligactis* an ideal model system in which to begin to test hypotheses about the role of bioelectrics in the aging process. However, the bioelectrics of whole-body immortal and aging hydra are unknown.

We established an imaging protocol for this species and tested the hypothesis that bioelectric patterns (nonhomogeneous spatial distributions of V_{mem}) would exist and would change with aging, especially becoming less crisp and more diffuse (degradation of prepattern as observed during some birth defects[72]). Moreover, we tested whether aging CS *H. oligactis* would be more or less hyperpolarized than immortal CS *H. oligactis*.

Methods

Hydra husbandry and shrimp maintenance

We obtained CS *H. oligactis* from Brigitte Galliot's Lab. We grew the hydra in media consisting of 0.294 g calcium chloride, 0.07 g magnesium sulfate, 0.08 g sodium bicarbonate ($NaHCO_3$), and 0.004 g potassium chloride per 2 L of deionized (DI) water. We stored the hydra in 150 × 15 mm plastic Petri dishes (maximum 50 hydra per dish) in a light: dark 16:8 h cycle incubator at 22°C. We transferred the hydra to a new Petri dish with fresh liquid approximately every 2 weeks. We grew artemia shrimps in a plastic cone oxygenated with an air pump in a light:dark 16:8 h cycle incubator at 22°C. The plastic cone had ∼300 mL of artemia brine shrimp media (25 g sodium chloride and 0.5 g $NaHCO_3$ per 1 L of DI) and 0.5 g of artemia brine shrimp egg microcysts.

We repeated the artemia brine shrimp growing process from artemia brine shrimp egg microcysts on Tuesdays and Fridays. We fed the hydra approximately one to four artemia brine shrimps per hydra on Mondays, Tuesdays, Thursdays, and Fridays.

Testing for potential dye toxicity

We tested whether the FluoVolt dye is toxic to the hydra by observing their survival and phenotype after dyeing. Specifically, we collected the hydra from the 22°C incubator. We used five hydra per condition. We imaged the hydra under the Nikon SMZ1500 stereoscope. Then, for the treatment condition, we used the following volumes per hydra: FluoVolt (0.5 μL), power load (12.5 μL), Neuro Background Suppressor 10× (12.5 μL), and hydra media (224.5 μL). For the control, we used the following volumes per hydra: power load (12.5 μL), Neuro Background Suppressor 10× (12.5 μL), and hydra media (225 μL). We placed a hydra in 250 μL of the (control or treatment) solution in a well of a 24-well plate. After 5 min, we washed the well approximately five times with hydra media using a different plastic pipette each time. We imaged the hydra again under the Nikon SMZ1500 stereoscope and then once every day for up to 4 days. During these 4 days, when the hydra were not imaged under the Nikon SMZ1500 stereoscope, they were kept in the 22°C incubator.

Aging induction

In the beginning of the experiment, after a month since the beginning, after 2 months since the beginning, and after 3 months since the beginning, we imaged four hydra from a culture growing at 22°C and four hydra from a culture growing at 10°C. After 4 months since the beginning of the experiment, we imaged eight hydra from the culture growing at 22°C and eight hydra from the culture growing at 10°C.

Dyeing and imaging the hydra

We performed the following steps in order to dye and image the hydra. We used fluorescence lifetime imaging microscopy (FLIM) as it allows imaging of the relative membrane voltage in live organisms[73] and does not rely on dye concentration versus other imaging techniques that rely on image intensity.[68] On the confocal microscope, we set the chamber temperature at 18°C and 40% air flow. We used the 25× objective (HC Fluotar L Visir 25×/0.95 water) with drops of ultrapure water on the objective. In the Leica Application Suite X (LASX) software, we used the following settings: 1024 × 1024 dimensions; bidirectional mode turned on; line accumulation: 9; speed: 700 Hz; numerical aperture: 0.95; WLL ON at 85% and maximum power; PinholeAiry: 1 AU; laser line (510 nm) and intensity 1.5%; spectral position: 528–617 nm; and gain = 10.

We prepared the dye solution for multiple hydras on the day of imaging using 2 mL Eppendorf tubes. Specifically, we used the following volumes per hydra: FluoVolt (https://www.thermofisher.com/order/catalog/product/F10488) (0.5 μL), power load (https://www.thermofisher.com/order/catalog/product/P10020) (12.5 μL), Neuro Background Suppressor 10× (12.5 μL), and hydra media (224.5 μL). We stored the Eppendorf tubes in the dark at room temperature until using

them for each hydra in the next few hours. We collected the hydra from the 22°C incubator and then once finished imaging the 22°C hydra, we imaged the hydra that were growing in the 10°C incubator. We placed a hydra in 250 μL of the dye solution in a well of a 24-well plate. We set a timer for 5 min. We then cut a cover slip on the sides so that it fitted in the middle of an ibidi dish (https://ibidi.com/35-mm-dishes/176-dish-35-mm-high-glass-bottom.html#/29-surface_modification-15h_170_m_5_m_d_263_m_schott_glass_sterilized/30-pcs_box-60_individually_packed). We placed molykote glue on two opposite sides of the ibidi dish (enough glue so that the cover slip could later touch on both sides of the glue). Once the 5 min had passed, we washed the well approximately five times with hydra media using a different plastic pipette each time. We collected the hydra with a plastic pipette and placed it in the middle of the ibidi dish. We placed the cover slip gently on top of the ibidi dish. We took a 10 μL tip with the ibidi dish to the confocal microscope. We placed some additional ultrapure droplets on the confocal 25× objective if needed, so that the liquid touched the bottom of the ibidi dish. We started applying pressure on the sides of the cover slip where the molykote glue had been applied until the glue did not visibly move much further toward the center of the ibidi dish. We made sure the molykote glue did not touch the hydra. We placed the ibidi dish on the confocal microscope stage. We switched the line repetitions on the LASX software to 1, went to tiling mode, and clicked on fast live. We focused on the surface of the hydra (which were not completely immotile) by adjusting the Z plane. We clicked on spiral and identified the whole body of the hydra. We stopped the spiral. Using the polygon tool, we selected the region of interest (the whole hydra). We turned the line repetitions to 9, clicked start, and on the image that was being processed, we clicked on the "Pixel binding" option to convert it to 2. For every image, we clicked on "fit," then "FLIM image fit," and used count threshold = 1. The maximum time that the hydra was being imaged under the confocal was 5 min. The pixel dwell time (i.e., how long the laser was on a single pixel) was 0.4–0.6 μs. If each micrometer is approximately 2 pixels, and the typical size of a hydra cell is 10–50 μm, then a cell would typically be imaged within $\sim$8–40 μs. It typically takes milliseconds for a neural or muscle cell to change its membrane potential and seconds (or minutes) for typical nonneural cells. Thus, a cell would be unlikely to have typically changed its membrane potential by the time the whole cell was being imaged. However, it might have changed its membrane potential by the time the whole frame of the tissue region was being imaged. Completion of a 1024 × 1024 pixel frame takes a few hundred milliseconds. Therefore, if it takes a few milliseconds for a cell to change its membrane potential, a cell might have changed its membrane potential by the time the entire frame has been completed. We then continued dyeing and imaging the next hydra.

Image analysis of the aging experiment

We obtained the mean lifetime intensity and brightness whole-body images of each FluoVolt-dyed hydra from the LASX software. We transferred these two images of each hydra on ImageJ. We also transferred and ran the following file (Supplementary Data S1) on ImageJ. Downloading this file (Supplementary Data S2) is also required. We then transferred and ran this file (Supplementary Data S3) on ImageJ.

In the case of the last file, we manually drew a line surrounding the hydra with the polygon tool. We used the rotation tool to rotate the hydra so that its anterior side was facing left and its posterior side was facing right. We then transferred and ran the following code on ImageJ (Supplementary Data S4). The output values from ImageJ were mean lifetime intensity values across the whole body of the hydra. We transferred these values to Excel, calculated the mean value of the mean lifetime intensity, and the first derivative of these values along the body of the hydra. We also measured the absolute value of the first derivative and the average of the absolute value of the first derivative. The output values from ImageJ also provided values of the x-axis (1 until the total length of the hydra). In order to normalize to the varied length of each hydra, we multiplied each position by 100/(the last × value of the hydra). For example, the last region of the hydra was the 100% region.

To compare the central region and foot region of the hydra, we removed the tentacles by not selecting the tentacles when drawing a line around the hydra on ImageJ. We used the mean lifetime intensity data from the output of this ImageJ analysis and we divided the mean lifetime intensity of the last four regions of each hydra ($\sim$83–100% of their body length) by the mean lifetime intensity of the region that was closest to 50% (of the body length of the hydra).

To measure bioelectric sharpness (Moran's *I*) of the whole body of the hydra, we transferred the mean lifetime intensity image of the hydra to ImageJ. We adjusted the brightness and contrast so that we could observe the edges of the hydra without applying those settings. Then we ran the following .lut file (Supplementary Data S2). Then, for each image, we cropped the region of interest (whole body of the hydra) using the polygon tool and ran the following macros (Supplementary Data S3). Then, we reset the brightness and contrast settings. We saved the image on the desktop as a TIFF format file. We then ran these two scripts (Supplementary Data S5 and S6) in Idle.[74]

Consensus bioelectric map of the hydra

To make a bioelectric atlas/map of every hydra, we analyzed separately the mean lifetime intensity whole-body data of the immortal hydra versus the mean lifetime intensity whole-body data of the old mortal hydra. We plotted the mean values of mean lifetime intensity of each hydra that was growing for 2 months (four hydra), 3 months (four hydra), and 4 months (eight hydra) at 22°C against the percentage of its body length on the x-axis and the mean values of mean lifetime intensity of each hydra that was growing for 2 months (four hydra), 3 months (four hydra), and 4 months (eight hydra) at 10°C against the percentage of its body length on the x-axis.

Image analysis of the VF2.0.Cl-dyed versus VF2.1.Cl-dyed versus FluoVolt-dyed hydra

We dyed 3 three-and-a-half-month-old hydra for 5 min with 250 μL of the following solution (1.5 μL of the VF2.1.Cl dye from a 1 mM stock solution,[75] 37.5 μL of power load, 37.5 μL of Neuro Background Suppressor 10×, and 673.5 μL of hydra media). We dyed 3 three-and-a-half-month-old hydra for 5 min with 250 μL of the following solution (1.5 μL of the VF2.0.Cl dye from a 1 mM stock

solution,[75] 37.5 μL of power load, 37.5 μL of Neuro Background Suppressor 10×, and 673.5 μL of hydra media). We dyed 3 three-and-a-half-month-old hydra for 5 min with 250 μL of the following solution (1.5 μL of the FluoVolt dye, 37.5 μL of power load, 37.5 μL of Neuro Background Suppressor 10×, and 673.5 μL of hydra media). We performed this procedure separately for each hydra. After the 5 min exposure to the dye in a well of a 24-well plate, we washed the well—four to five times with hydra media. We placed molykote glue on two opposite sides of an ibidi dish and moved the hydra with a plastic pipette to the middle of the ibidi dish. We slowly applied pressure on the sides of the cover slip where the molykote glue was, and imaged the hydra under the confocal microscope using the LASX software and the 25× objective. We used the following settings for all three dyes: 1024 × 1024 dimensions; bidirectional mode turned on, line accumulation: 9; speed: 700 Hz; numerical aperture: 0.95; WLL ON at 85% and maximum power; and PinholeAiry: 1 AU. For imaging the FluoVolt-dyed hydra, we used laser line (510 nm) and intensity 1.5%; spectral position: 528–617 nm; and gain = 10, whereas for imaging the VF2.1.Cl- and VF2.0.Cl-dyed hydra, we used laser line (510 nm) and intensity 30%; spectral position: 533–622 nm; and gain = 10. On the images that were being processed, we clicked on the "Pixel binding" option to convert it to 2. Also, for every image we clicked on "fit," then "FLIM image fit," and used count threshold = 1.

We obtained the mean lifetime intensity and brightness whole-body images of the VF2.0.Cl-, VF2.1.Cl-dyed, and FluoVolt-dyed hydra from the LASX software. We dragged these images on the ImageJ software. In the brightness image of each hydra, we looked for six neighboring cells in the foot region and drew a circle around them in the mean lifetime intensity image to measure the average mean lifetime intensity of that region. We also found six neighboring cells from the middle region of the brightness image of the hydra with a maximum ±1 difference in brightness intensity. We drew a circle around those cells in the same position in the mean lifetime intensity image in order to measure the average mean lifetime intensity of those cells. We then compared the average mean lifetime intensity values of those two regions across the different conditions (VF2.0.Cl-dyed vs. VF2.1.Cl-dyed vs. FluoVolt-dyed hydra).

Statistical analyses

We performed all statistical analyses in R version 4.4.0.[76] When the data followed an approximately normal distribution (p value >0.05 in Shapiro's test[77]) and we were comparing three or more different groups, we used an analysis of variance test. If the data did not follow a normal distribution (p value <0.05 in Shapiro's test[77]) and we were comparing three or more different groups, we performed the Kruskal–Wallis test.[78] When the data did not follow a normal distribution (p value >0.05 in Shapiro's test[77]) and we were comparing two different groups, we performed the Wilcoxon rank-sum exact test.[79,80]

Results

Hydra survive the dyeing protocol with no consistent deformities

In order to test whether the FluoVolt dye that we used is toxic to the hydra, we compared the survival and phenotypes

of hydra exposed to FluoVolt + power load + Neuro Background Suppressor 10× + hydra media versus power load + Neuro Background Suppressor 10× + hydra media. We used five hydra per condition and found no death or consistent large-scale visible deformities in the two conditions throughout 4 days after the exposure to the solution (Supplementary Fig. S3 and Fig. S4). One of the hydra that was exposed to the FluoVolt-containing solution had tentacles prior to staining and 1, 2, and 4 days after staining, but did not have clearly visible tentacles 3 days after staining (top row; Supplementary Fig. S4), either because it had no tentacles on that day or because they had contracted and were behind the anterior region of the hydra and thus were not visible in the 2D image. Another hydra that was exposed to the FluoVolt-containing solution had a circular structure in its gastric cavity only on the second day after exposure to the FluoVolt-containing solution, but not prior to exposure, just after exposure, or on the first, third, or fourth day after exposure to the FluoVolt-containing solution (bottom row; Supplementary Fig. S4). It is not clear whether this circular structure formed due to the dye or due to other reasons, as this circular structure did not appear in any of the other replicates or on any of the other days of imaging. These results show that these two solutions are not life-threatening for the hydra and do not cause deformities across replicates throughout 4 days after exposure.

V_{mem}-sensitive dye reveals relative membrane voltage of every cell along the hydra's body

In order to determine whether we can use immortal and mortal hydra as a model system to see the relative membrane voltage of every cell, we ran an imaging protocol with the V_{mem}-sensitive dye FluoVolt. We were able to see the relative membrane voltage of every cell in living immortal and mortal hydra (Supplementary Fig. S1). Depending on the hydra's body contraction or expansion at the exact time point of imaging, some cells appeared more elongated (e.g., anterior-right region of the hydra in Supplementary Fig. S1A), while other cells appeared less elongated (e.g., anterior-right region of the hydra in Supplementary Fig. S1B). Therefore, our dyeing technique can reveal the whole-body bioelectric atlas of immortal and mortal hydra.

V_{mem}-sensitive dyes FluoVolt and VF2.1.Cl show relative membrane voltage and not artifacts

In order to test whether the V_{mem}-sensitive dyes FluoVolt and VF2.1.Cl do report relative membrane voltage of hydra cells, we compared the average arrival time of old mortal hydra dyed with FluoVolt, VF2.1.Cl, or the V_{mem}-insensitive dye VF2.0.Cl. Arrival time refers to the time difference between the excitation of the fluorophore by the laser pulse and the arrival of the emitted photon at the detector.[81] For example, in the case of V_{mem}-sensitive dyes, longer arrival time indicates a relatively hyperpolarized cell membrane, whereas shorter arrival time indicates a relatively depolarized cell membrane. In old mortal hydra dyed with FluoVolt ($N = 3$) or VF2.1.Cl ($N = 3$), we saw that the average arrival time of the foot region was longer than the average arrival time of the central body region. However, in old mortal hydra dyed with the V_{mem}-insensitive dye VF2.0.Cl ($N = 3$), the foot and central body regions had, on average, a similar
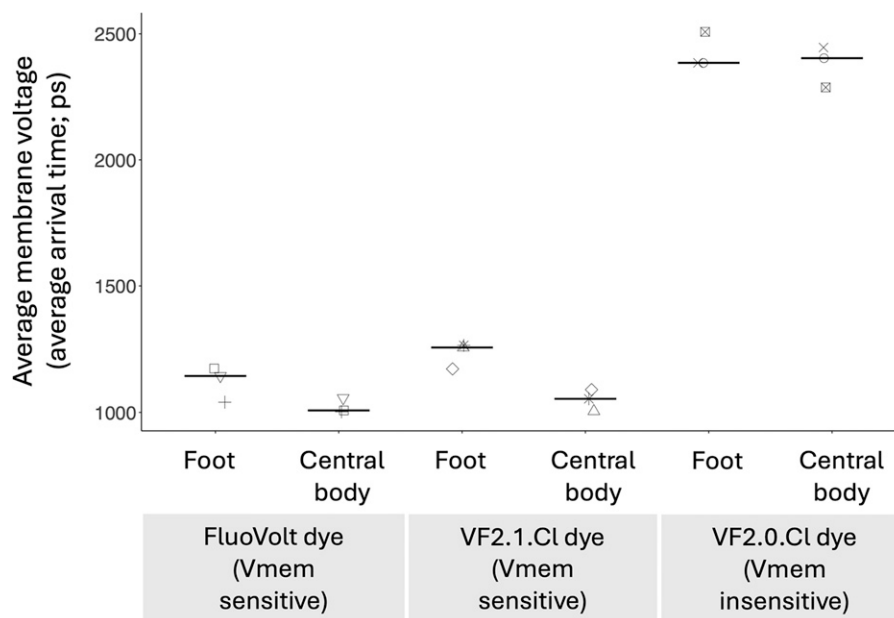
FIG. 1. The V_{mem}-sensitive dyes FluoVolt and VF2.1.Cl show membrane voltage, rather than V_{mem}-insensitive artifacts. The y-axis shows the mean membrane voltage in the foot or central body regions of three-and-a-half-month-old hydra that have been growing at 10°C, dyed with the FluoVolt dye + power load + Neuro Background Suppressor, VF2.1.Cl dye + power load + Neuro Background Suppressor, or VF2.0.Cl dye + power load + Neuro Background Suppressor. The foot is relatively more depolarized than the middle part of the hydra's body when using the V_{mem}-sensitive dyes, but not when using the V_{mem}-insensitive dye. Same shapes are from the same hydra. There are three different hydra per dye condition. Crossbars show median values. ps, picoseconds.

average arrival time (Fig. 1). The absence of the characteristic voltage pattern when using the closely related but voltage-unresponsive VF2.0.Cl dye suggests that the signals we reported indeed show relative membrane voltage of hydra cells and are unlikely to be due to artifacts unrelated to voltage.

Immortal hydra have bioelectrically distinct body parts

In order to find the consensus bioelectric atlas of immortal hydra, we imaged hydra growing at 22°C with the V_{mem}-sensitive dye FluoVolt. We saw that the majority of immortal hydra had a depolarized foot. Some immortal hydra had depolarized tentacles. Other regions of the immortal hydra did not have such consistent membrane voltage among different individuals. For example, the mouth region and central body of the hydra varied in membrane voltage among the different individuals (Fig. 2; $N = 6$). Therefore, the consensus whole-body bioelectric atlas of immortal hydra showed some consistently bioelectrically distinct regions, such as the depolarized foot, and some bioelectrically variable regions, such as the depolarized tentacles, the mouth, and central body.

Hydra age at 10°C

In order to confirm whether hydra age at 10°C, we looked for ovaries or testes on the body of the hydra since gametogenesis in these hydra is a sign of irreversible aging.[70,82] Hydra that had been growing for 78 days at 10°C had visible ovaries/testes (Supplementary Fig. S2). Therefore, we conclude that in our assays, hydra do indeed age at 10°C.

Aging hydra have bioelectrically different bodies than immortal hydra

In order to test whether aging and immortal hydra have bioelectrically distinct bodies, we grew cultures of hydra in 10°C versus 22°C incubators for 4 months and imaged the relative membrane voltage across the hydras' bodies using the V_{mem}-sensitive dye FluoVolt. The technical replicates, that is, two whole-body images from the same individual, varied in mean lifetime intensity (Table 1). Both groups, the technical replicates of the immortal and old mortal hydra, had similar standard deviations (Table 1: 4–46 ps in the case of immortal hydra and 4–47 ps in the case of old mortal hydra). By analyzing one image of the whole body of each hydra, the standard deviation among the biological replicates of Figures 3 and 4A was 101 picoseconds in the case of immortal hydra and 79 picoseconds in the case of old mortal hydra. We saw that the bodies of old mortal hydra, which had been growing for 2, 3, or 4 months at 10°C, were on average more hyperpolarized ($N_{immortal} = 16$, $N_{old\ mortal} = 16$; Figs. 3 and 4A: $p < 0.0001$) and bioelectrically sharper ($N_{immortal} = 16$, $N_{old\ mortal} = 16$; Fig. 4B; $p = 0.03$) than immortal hydra, which had been growing for 2, 3, or 4 months at 22°C. The foot-to-central body ratio of old mortal hydra was not as bioelectrically sharp as that of immortal hydra ($N_{immortal} = 16$, $N_{old\ mortal} = 16$; Fig. 5; $p = 0.01$). Therefore, the bodies of old mortal and immortal hydra have distinct average relative membrane voltage and sharpness of different body regions.

Discussion

This study provides a consensus whole-body bioelectric atlas of living immortal and mortal hydra. We confirmed that
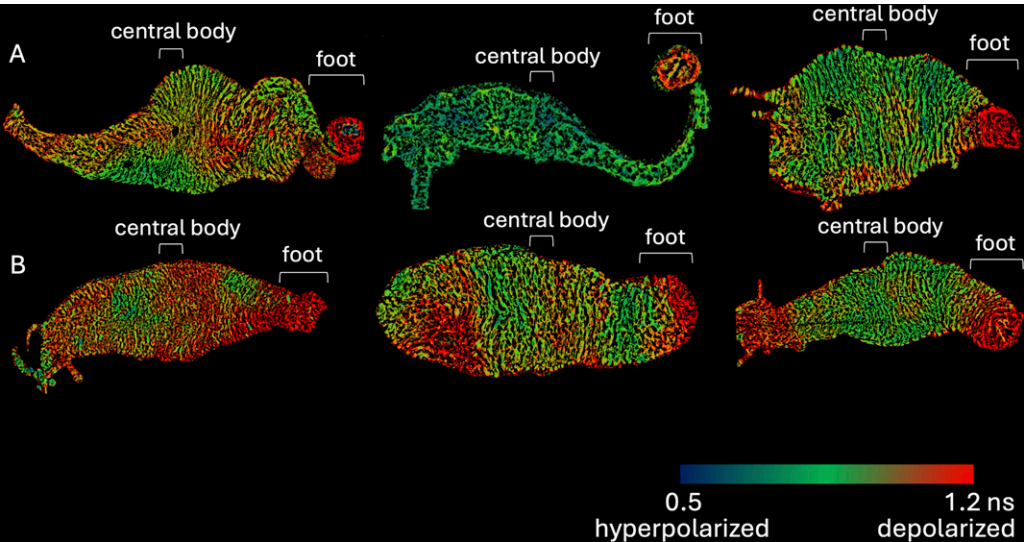
FIG. 2. The bioelectric atlas of different individual immortal hydra shows a common feature: a relatively depolarized foot and occasionally depolarized tentacles. Examples of the relative membrane voltage of **(A)** three young hydra at 22°C and **(B)** three young 3-month-old hydra at 22°C. Relative membrane voltage is observed using the FluoVolt dye. Mean lifetime intensity (nanoseconds) ranges from low (blue; hyperpolarized) to high (red; depolarized) values. Images were analyzed in ImageJ software. We aligned the hydra so that their anterior is on the left and their posterior end is on the right.

hydra were aging at 10°C since they had formed ovaries/testes within 78 days, an indication that this strain is undergoing irreversible aging.[70,82]

Our results showed that in this model system, the FluoVolt and VF2.1.Cl dyes were showing V_{mem} of the plasma membrane and not artifacts, as revealed by the lack of signal from a closely related control dye that is not responsive to membrane potential. This control has been used in cultures of rat hippocampal neurons, human cardiomyocytes, human embryonic kidney cells,[83–85] and the tails of living frog embryos,[68] but is not common and should be universally used in voltage dye studies.

Prior efforts have mapped action potentials of the anterior region of the guinea pig's heart[86,87]; resting potential patterns in bacterial biofilms[88]; central regions of poplar leaves[89] and stem and leaf of sunflowers *Helianthus annuus*[90]; the optic tectum region of the frog brain[91]; the olfactory bulb of the salamander *Ambystoma tigrinum*[92,93]; faces, brains, and tails of frog embryos[30,68,72]; olfactory bulb of zebrafish[94,95]; olfactory bulb of box turtles *Terrapene triunguis*[96]; an embryonic precontractile chick heart[97]; the pig heart[98]; mouse heart[87,99]; and the primary somatosensory cortex of the mouse brain.[100] We show for the first time the relative membrane voltage of living cells across the whole body of 38 whole organisms. Certain properties of hydra and technological advances have made this possible. Specifically, hydra has a very thin layer of cells, and thus V_{mem}-sensitive dyes can easily penetrate these cell layers and be observed under the confocal microscope using FLIM that shows the relative membrane voltage of each cell.

A limitation to note in our data is that we cannot rule out changes in membrane voltage of cells that change their

TABLE 1. TECHNICAL REPLICATES FROM THE SAME INDIVIDUAL VARY IN THEIR BIOELECTRICS

	Mean lifetime intensity (picoseconds)		Standard deviation (picoseconds) among the two technical replicates	Time interval (minutes) between the first and second technical replicate
Individual	*First technical replicate*	*Second technical replicate*		
First immortal hydra	1009	1074	45.96	3
Second immortal hydra	1066	1125	41.72	3
Third immortal hydra	1061	1040	14.85	1
Fourth immortal hydra	1124	1129	3.54	3
First old mortal hydra	1000	935	45.96	2
Second old mortal hydra	1003	977	18.38	3
Third old mortal hydra	1008	1013	3.54	1
Fourth old mortal hydra	959	893	46.67	2

These are examples of mean lifetime intensity values from technical replicate images of the whole body of four immortal hydra (4 months post-experimental induction at 22°C) and four old mortal hydra (4 months post-experimental induction at 10°C). Higher mean lifetime intensity values indicate relative depolarization, whereas lower mean lifetime intensity values indicate relative hyperpolarization. Longer duration of the hydra under the cover slip, that is, longer time interval between the first and second technical replicate, was not consistently an indication of depolarization or hyperpolarization.
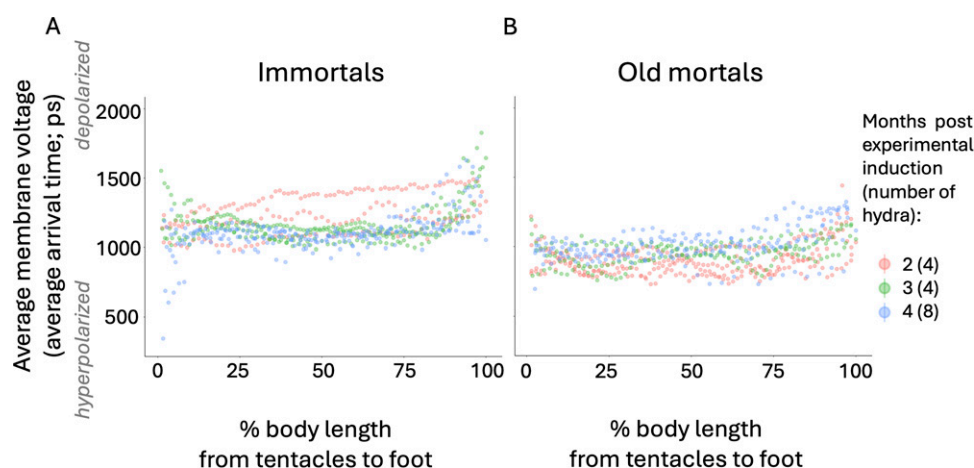
FIG. 3. The bioelectric atlas of 16 immortal hydra **(A)** is more depolarized on average, in the foot region, and occasionally in the tentacles in comparison to the bioelectric atlas of 16 old mortal hydra **(B)**. **A** and **B** have the same axes ranges. The mean lifetime intensities of the whole body of immortal hydra were not statistically different (Kruskal–Wallis test: p value >0.05) after 2 months (four hydra), 3 months (four hydra), or 4 months (eight hydra). Therefore, we show the mean lifetime intensity (**A**: y-axis) from anterior to posterior (**A**: x-axis) of these 16 different immortal hydra. The mean lifetime intensities of the whole body of old mortal hydra were not statistically different (ANOVA: p value >0.05) after 2 months (four hydra), 3 months (four hydra), or 4 months (eight hydra); therefore, **B** shows the means of those 16 old mortal hydra. Therefore, we show the mean lifetime intensity (**B**: y-axis) from anterior to posterior (**B**: x-axis) of these 16 different old mortal hydra. ANOVA, analysis of variance; ps, picoseconds.

membrane voltage faster (within approximately a few milliseconds[101]) than the completion of the whole-body imaging of a hydra (a few hundred milliseconds: see the section "Methods"). Such signals are unlikely to be critical for developmental bioelectricity because the transduction machinery – and downstream effects on transcriptional changes, epigenetic processes, and cell behavior – all typically take minutes to hours to take place.[102]

With any dye, it is important to consider potential toxicity. We do not believe this was a factor in our study. Regarding potential dye toxicity, any dye toxicity would be present in both hydra conditions, and in the old mortal versus immortal hydra analyses, we are reporting differences in the relative bioelectric pattern of these two conditions that have both been exposed to the dye and washed using the same protocol. The hydra were alive after the brief exposure to the dye, and when they were imaged under the confocal. The laser line used to image the hydra was in the green region (510 nm) and thus relatively less cytotoxic than if a laser line in the blue region was used.[68] If the dye was toxic, we would expect the entire body of the hydra to be depolarized; however, the hydra's body was not entirely depolarized. Also, Miller et al. have found that VoltageFluor dyes have almost no capacitance compared with other V_{mem} sensors, so they have relatively little effect on V_{mem}.[75] Additionally, exposure to the FluoVolt dye did not affect survival of the hydra or consistently change the morphology of the hydra 4 days after exposure to the dye (Supplementary Fig. S3 and Fig. S4)—a much longer time period than the minutes timescale on which we stained and imaged.

One of the key aspects of bioelectric patterns is that in some systems (*Xenopus* embryo, regenerating planaria, chick embryo), their distribution has been shown to serve as an instructive signal for morphogenesis.[30,103–106] Thus, we were very interested in differences in V_{mem} across the hydra

that would correspond to distinct anatomical features. We found that the foot of the hydra was more depolarized than other regions of the hydra's body. The tentacles of the hydra were also relatively depolarized in some individuals. This relative depolarization may relate to the adhesive properties of the foot and secretory properties of the hydra's tentacles. The hydra's foot (also called basal disc) secretes granules that contain glycans and/or glycoproteins, allowing the hydra to stick on surfaces.[107] Although the resting membrane potential of the secretory cells of the foot has not been previously reported, other secretory cells, called nematocytes, in the tentacles of *Hydra vulgaris* are known to require apical plasma membrane depolarization for the secretion of stenoteles.[108]

As with any biological parameter, we observed some variability across animals. The standard deviation in mean lifetime intensity was higher among the biological than among the technical replicates. Specifically, the standard deviation in mean lifetime intensity among the biological replicates of the data shown in Figure 3 and Figure 4A was 101 and 79 picoseconds in the case of the immortal hydra and old mortal hydra, respectively; whereas the standard deviation in mean lifetime intensity among the technical replicates ($N = 2$; Table 1) was 4–46 ps in the case of four immortal hydra and 4–47 ps in the case of four old mortal hydra. Although the standard deviation in mean lifetime intensity of the technical replicates was only measured from two technical replicates, the higher standard deviation in the case of the biological replicates compared to that of the technical replicates indicates that each hydra does not have the same whole-body mean lifetime intensity as other hydra. There tends to be more interindividual variation in the bioelectric pattern of hydra than temporal (1–3 min) variation in the bioelectric pattern of a single individual. In other words, the lower standard deviation in the case of the technical replicates,

A

P-value = 0.000001

B

P-value = 0.03
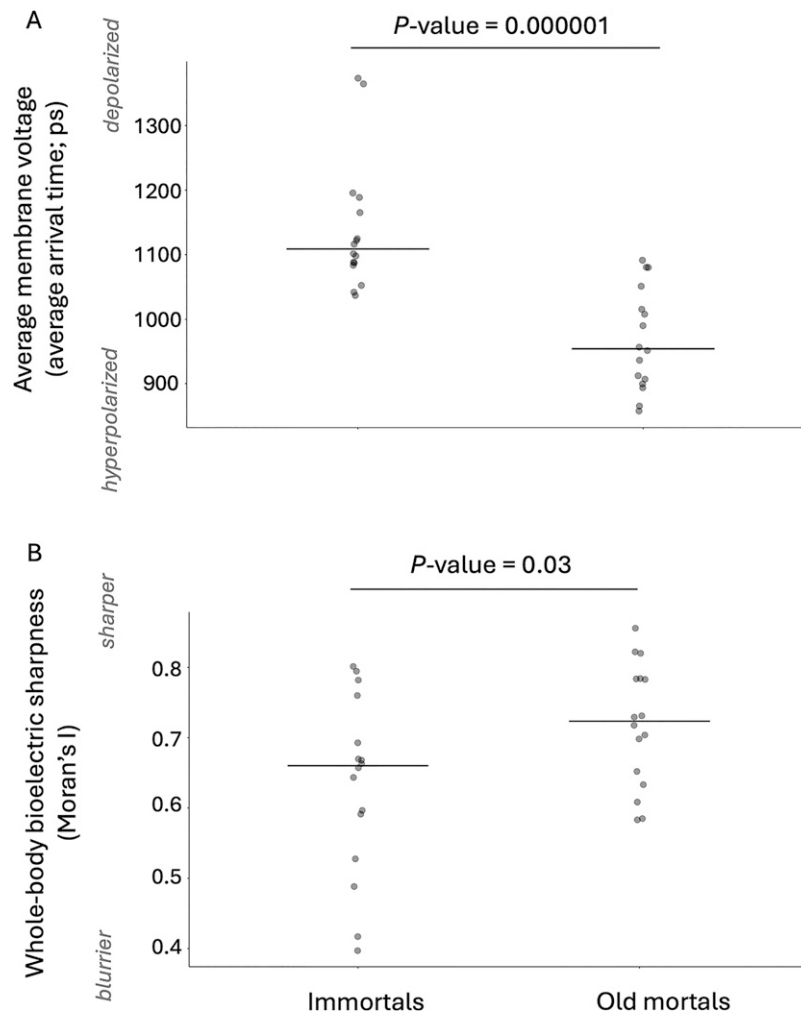
FIG. 4. The whole body of 16 old mortal hydra is, on average, more hyperpolarized **(A)** and bioelectrically sharper **(B)** than 16 immortal hydra. **(A)** Average arrival time (ps) of the whole body of old mortal hydra (growing for 2, 3, or 4 months at 10°C; nonstatistically significant difference between the average arrival time values between these three time points; ANOVA test: *p* value >0.05) versus immortal hydra (growing for 2, 3, or 4 months at 22°C; nonstatistically significant difference between the average arrival time values between these three time points; Kruskal–Wallis test: *p* value >0.05). Sharpness **(B)** of the whole body of old mortal hydra (growing for 2, 3, or 4 months at 10°C; nonstatistically significant difference between Moran's *I* values at these three time points; ANOVA test: *p* value >0.05) versus immortal hydra (growing for 2, 3, or 4 months at 22°C; nonstatistically significant difference between Moran's *I* values at these three time points; ANOVA test: *p* value >0.05). Each point is a different hydra. The hydra were dyed with the membrane voltage dye: FluoVolt. We only show *p* values that are statistically different (*p* value <0.05). Result of Wilcoxon signed-rank exact test **(A)**: $W = 242$, *p* value = 1.69×10^{-6}. Result of independent-samples *t* test **(B)**: df = 26.7; *p* value = 0.0374. The crossbars show medians. ANOVA, analysis of variance; ps, picoseconds.

versus biological replicates, indicates that data within the ~4–47 ps standard deviation could be considered temporal intraindividual variation ("noise") and data beyond the ~47 ps standard deviation could be considered interindividual variation ("signal"). Future work on the functional role of this parameter in hydra biology will be necessary because it is the precision of interpretation of the voltage profile by body systems that would determine the degree of precision that is physiologically important.

One basic bioelectric parameter to compare in living samples is simply the overall average level of polarization. With respect to this, we found a more hyperpolarized bioelectric pattern in the whole body of 2- to 4-month-old mortal than

in immortal hydra. The difference cannot be due to temperature per se since we collected all voltage data at the same temperature. What we observed may be due to dynamic changes among many different types of interacting cells. To be more specific, what we found was reasonable for two reasons. First, we would expect the immortal hydra's foot and tentacles to be relatively depolarized, due to the depolarization required for excretion of substances in secretory cells present in those regions. If this depolarization becomes dysregulated during aging, we would expect old hydra to be, on average, more hyperpolarized than immortal hydra. Second, hyperpolarization of the plasma membrane is known to determine actin fiber compaction in cultures of bovine
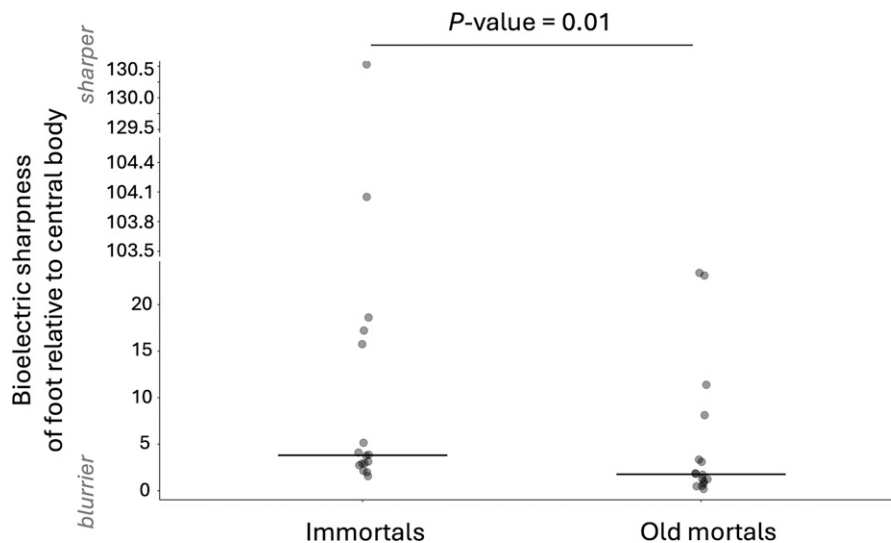
FIG. 5. The hydra's foot (relative to the bioelectric sharpness of its central body region) loses its bioelectric sharpness with age. Each point is a different hydra. Sharpness of the foot relative to the central body of old mortal hydra (growing for 2, 3, or 4 months at 10°C; nonsignificant difference between the y values at these time points; Kruskal–Wallis test: p value >0.05) versus immortal hydra (growing for 2, 3, or 4 months at 22°C; nonsignificant difference between the y values at these time points; Kruskal–Wallis test: p value >0.05). The y-axis is the median of the bioelectric sharpness of the foot region ($\sim$83–100% of the hydra, where 100% is the edge of the foot) divided by the mean bioelectric sharpness of the middle region ($\sim$50% position of body length of the hydra). The sharpness of the bioelectric pattern is the absolute value of the first derivative (of the mean lifetime intensity). Result of Wilcoxon rank-sum exact test: $W = 190$, p value = 0.01893. After removing the statistically significant outliers (Rosner's test), the statistical significance remains (two-sample t test: $t = 3.9266$; df = 21; p value = 0.0007). The crossbars show medians.

epithelial cells,[109] and actin fibers appear disrupted in aging hydra.[71] Thus, although these two processes happen in very evolutionary distant species, the disrupted actin fibers of aging hydra may be due to cell hyperpolarization.

There seems to be some variety across organisms in terms of the relationship of polarization level to aging. For example, Type II neurons in the bed nucleus of the stria terminalis are more hyperpolarized in aged mice than in young mice.[110] In rats, old versus young hippocampal CA1 neurons did not have significantly different resting membrane potentials.[111] Also, there was no significant difference in the resting membrane potential of old versus young pyramidal neurons of the prefrontal cortex of rhesus monkeys.[112] In female and male mouse bladder cells, the messenger RNA expression of the *hcn1* gene, which encodes the hyperpolarization-activated cyclic nucleotide-gated (HCN) channel, decreases with age.[113] *H. vulgaris* also has HCN channels (https://www.ncbi.nlm.nih .gov/gene/100208250; https://www.ncbi.nlm.nih.gov/gene/ 105844959) which are approximately 1 substitution per site, on the protein sequence, different than the human HCN1-4 channels.[114] If *hnc1* expression is lower and production of HCN1 proteins is decreased in aging hydra, this may explain the potential inability of cells to maintain their depolarized state as they age, that is, our finding that older mortal hydra are more hyperpolarized than immortal hydra.

In addition to average polarization, it is interesting to consider the crispness of the bioelectric pattern itself: the degree to which bioelectric patterns sharply distinguish compartments with different V_{mem}.[22,115] In embryos, a number of teratogens that disrupt developmental morphogenesis do so by making the bioelectric prepattern less sharp.[72,116] For example, in the *Xenopus* brain, this is known to be the case for chemical and genetic teratogens; crucially, brain morphogenesis, gene expression, and even learning rates can be restored despite exposure to nicotine, ethanol, or mutation of the Notch gene by artificially forcing the bioelectric pattern to become sharper (via overexpression of *hcn2*, which encodes an ion channel).[117–119] We previously suggested the hypothesis that aging could involve a change of the sharpness of the bioelectrical pattern[25] and indeed *hcn1* expression decreases with age in mice.[113] We thus quantified here the sharpness of the bioelectrical patterns in immortal and aging hydra. We found a sharper bioelectric pattern in the whole body of old mortal than immortal hydra. However, the foot-to-central body ratio pattern was less sharp in the old mortal hydra. This suggests either that different organisms handle this in different ways, or more likely, that the relationship between crispness of V_{mem} pattern and aging is not uniform across body regions.

Our work points to the need for numerous subsequent studies. In parallel with applying antiaging bioelectric treatments (e.g., *hcn2* overexpression) in hydra, it would be useful to understand the mechanisms underpinning the observed whole-body bioelectric atlas of hydra. What ion channels and pumps determine the membrane voltage of every cell? Are there particular groups of cells that have more coordinated/synchronized changes in membrane voltage than other more distant groups of cells in the hydra's body? How exactly are the known aging-related physiologies of hydra (decreased ability to capture prey, decreased ability to spontaneously contract and transfer food to the gut, fewer sperm and nurse cells after 2 months, fewer interstitial stem cells, and fewer epithelial cells[71]) associated with the bioelectric atlas of old mortal hydra? Relative hyperpolarization of the old hydra's body may also mean a hyperpolarization of the depolarization-activated

nematocytes in the hydra's tentacles, thus contributing to their decreased ability to capture food. However, the associations between the other old physiologies and the old mortal bioelectric atlas are largely unknown. The availability of protocols for generating transgenic hydra[120–123] suggests the possibility of using optogenetics and ion channel misexpression to understand the role of bioelectrics in hydra morphogenesis and aging. Likewise, it would be interesting to understand the role, if any, of endogenous bioelectrical states and the abilities of external alternating electric fields to induce reversal and continuation of hydra morphogenesis.[124] Finally, since applied electric fields have been shown to induce reversible changes in hydra morphogenesis,[124,125] the future study of bioelectrics in various aspects of hydra biology is likely to reveal much of interest.

Identification of the whole-body bioelectric atlas of immortal and aging mortal hydra is a step toward performing similar studies in other model and nonmodel organisms. Studying the bioelectrics of aging in different taxa across the tree of life and the evolution of bioelectric pathways will help better understand the bioelectrics of aging in clinical settings. Examining the bioelectrics of human cells and tissues in both young and elderly populations would be essential in designing best practices for early human clinical trials using morphoceuticals[25] or gero-electroceuticals,[38] that is, drugs that target cellular bioelectrics and aim to reverse aging and aging-related diseases. Comparative developmental electrophysiology across widely distributed phyla is a first step in cracking the bioelectric code toward a better understanding of evolutionary physiology and the biomedicine of aging and disease.

Acknowledgments

Authors' Contributions

S.E.K.: Conceptualization, data curation, supervision, software, formal analysis, validation, visualization, investigation, methodology, project administration, writing—original draft, and writing—review and editing. A.P.: Data curation and investigation. P.M.: Supervision, software, project administration, data curation, resources, visualization, investigation, methodology, and writing—review and editing. P.T. and P.E.: Supervision. M.L.: Conceptualization, supervision, resources, funding acquisition, project administration, visualization, methodology, and writing—review and editing.

Author Disclosure Statement

M.L.'s lab has a sponsored research agreement with Astonishing Labs, a company seeking to advance the biomedicine of aging. All the other authors have no conflicts of interest to disclose.

Funding Information

Supplementary Material

Supplementary Data S1
Supplementary Data S2
Supplementary Data S3
Supplementary Data S4
Supplementary Data S5
Supplementary Data S6
Supplementary Figure S1
Supplementary Figure S2
Supplementary Figure S3
Supplementary Figure S4

References

1. Akushevich I, Kravchenko J, Akushevich L, et al. Medical cost trajectories and onsets of cancer and noncancer diseases in US elderly population. Comput Math Methods Med 2011;2011:857892; doi: 10.1155/2011/857892

2. Akushevich I, Kravchenko J, Arbeev KG, et al. Medical cost trajectories and onset of age-associated diseases. In: Biodemography of Aging. Yashin AI, Stallard E and Land KC, eds. Springer: Dordrecht; 2016; pp. 143–162.

3. Sousounis K, Baddour JA, Tsonis PA. Aging and regeneration in vertebrates. Curr Top Dev Biol 2014;108:217–246; doi: 10.1016/B978-0-12-391498-9.00008-5

4. Miller WB, Jr, Baluška F, Reber AS, et al. Why death and aging? All memories are imperfect. Prog Biophys Mol Biol 2024;187:21–35; doi: 10.1016/j.pbiomolbio.2024.02.001

5. Rubin H, Yao A, Chow M. Neoplastic development: Paradoxical relation between impaired cell growth at low population density and excessive growth at high density. Proc Natl Acad Sci U S A 1995;92(17):7734–7738; doi: 10.1073/pnas.92.17.7734

6. Rubin H. Mechanisms for enduring biological change. Am J Physiol 1992;262(1 Pt 1):L111–L113; doi: 10.1152/ajplung.1992.262.1.L111

7. Rubin H. What keeps cells in tissues behaving normally in the face of myriad mutations? Bioessays 2006;28(5):515–524; doi: 10.1002/bies.20403

8. Li S, Vazquez JM, Sudmant PH. The evolution of aging and lifespan. Trends Genet 2023;39(11):830–843; doi: 10.1016/j.tig.2023.08.005

9. Frankel S, Rogina B. Evolution, chance, and aging. Front Genet 2021;12:733184; doi: 10.3389/fgene.2021.733184

10. Meyer DH, Schumacher B. Aging clocks based on accumulating stochastic variation. Nat Aging 2024;4(6):871–885; doi: 10.1038/s43587-024-00619-x

11. Gems D, Singh Virk R, de Magalhães JP. Epigenetic Clocks and Programmatic Aging. 2023; doi: 10.20944/preprints202312.1892.v1

12. de Magalhães JP. Programmatic features of aging originating in development: Aging mechanisms beyond molecular damage? FASEB J 2012;26(12):4821–4826; doi: 10.1096/fj.12-210872

13. Gladyshev VN. On the cause of aging and control of lifespan: Heterogeneity leads to inevitable damage accumulation, causing aging; control of damage composition and rate of accumulation define lifespan. Bioessays 2012;34(11):925–929; doi: 10.1002/bies.201200092

14. Gladyshev VN, Kritchevsky SB, Clarke SG, et al. Molecular damage in aging. Nat Aging 2021;1(12):1096–1106; doi: 10.1038/s43587-021-00150-3

15. Yang JH, Hayano M, Griffin PT, et al. Loss of epigenetic information as a cause of mammalian aging. Cell 2024; 187(5):1312–1313; doi: 10.1016/j.cell.2024.01.049

16. Lu YR, Tian X, Sinclair DA. The information theory of aging. Nat Aging 2023;3(12):1486–1499; doi: 10.1038/s43587-023-00527-6

17. Szilard L. On the nature of the aging process. Proc Natl Acad Sci U S A 1959;45(1):30–45; doi: 10.1073/pnas.45.1.30

18. de Magalhães JP. Ageing as a software design flaw. Genome Biol 2023;24(1):51; doi: 10.1186/s13059-023-02888-y

19. Jin K. Modern biological theories of aging. Aging Dis 2010;1(2):72–74.

20. Lipsky MS, King M. Biological theories of aging. Dis Mon 2015;61(11):460–466; doi: 10.1016/j.disamonth.2015.09.005

21. Gems D. The hyperfunction theory: An emerging paradigm for the biology of aging. Ageing Res Rev 2022;74:101557; doi: 10.1016/j.arr.2021.101557

22. Levin M. Bioelectric signaling: Reprogrammable circuits underlying embryogenesis, regeneration, and cancer. Cell 2021;184(8):1971–1989; doi: 10.1016/j.cell.2021.02.034

23. Bates E. Ion channels in development and cancer. Annu Rev Cell Dev Biol 2015;31:231–247; doi: 10.1146/annurev-cellbio-100814-125338

24. Harris MP. Bioelectric signaling as a unique regulator of development and regeneration. Development 2021;148(10):dev180794; doi: 10.1242/dev.180794

25. Pio-Lopez L, Levin M. Aging as a loss of morphostatic information: A developmental bioelectricity perspective. Ageing Res Rev 2024;97:102310; doi: 10.1016/j.arr.2024.102310

26. Burr HS. The Problems of Ageing. Yale J Biol Med 1939; 11:690–691.

27. Weiß I, Bohrmann J. Electrochemical patterns during *Drosophila* oogenesis: Ion-transport mechanisms generate stage-specific gradients of pH and membrane potential in the follicle-cell epithelium. BMC Dev Biol 2019;19(1):12; doi: 10.1186/s12861-019-0192-x

28. Krüger J, Bohrmann J. Bioelectric patterning during oogenesis: Stage-specific distribution of membrane potentials, intracellular pH and ion-transport mechanisms in *Drosophila* ovarian follicles. BMC Dev Biol 2015;15:1; doi: 10.1186/s12861-015-0051-3

29. Adams DS, Uzel SG, Akagi J, et al. Bioelectric signalling via potassium channels: A mechanism for craniofacial dysmorphogenesis in KCNJ2-associated Andersen–Tawil Syndrome. J Physiol 2016;594(12):3245–3270; doi: 10.1113/JP271930

30. Vandenberg LN, Morrie RD, Adams DS. V-ATPase-dependent ectodermal voltage and pH regionalization are required for craniofacial morphogenesis. Dev Dyn 2011;240(8):1889–1904; doi: 10.1002/dvdy.22685

31. Chernet BT, Levin M. Transmembrane voltage potential is an essential cellular parameter for the detection and control of tumor development in a *Xenopus* model. Dis Model Mech 2013;6(3):595–607; doi: 10.1242/dmm.010835

32. Perez FP, Zhou X, Morisaki J, et al. Engineered repeated electromagnetic field shock therapy for cellular senescence and age-related diseases. Rejuvenation Res 2008;11(6):1049–1057; doi: 10.1089/rej.2008.0793

33. Xu J, Liu K, Chen T, et al. Rotating magnetic field delays human umbilical vein endothelial cell aging and prolongs the lifespan of *Caenorhabditis elegans*. Aging (Albany NY) 2019;11(22):10385–10408; doi: 10.18632/aging.102466

34. Marędziak M, Tomaszewski K, Polinceusz P, et al. Static magnetic field enhances the viability and proliferation rate of adipose tissue-derived mesenchymal stem cells potentially through activation of the phosphoinositide 3-kinase/Akt (PI3K/Akt) pathway. Electromagn Biol Med 2017;36(1):45–54; doi: 10.3109/15368378.2016.1149860

35. Li S, Tang Y, Zhou Y, et al. Effects of transcranial direct current stimulation on cognitive function in older adults with and without mild cognitive impairment: A systematic review and meta-analysis of randomized controlled trials. Gerontology 2024;70(5):544–560; doi: 10.1159/000537848

36. Chen J, Wang Z, Chen Q, et al. Transcranial direct current stimulation enhances cognitive function in patients with mild cognitive impairment and early/mid Alzheimer's disease: A systematic review and meta-analysis. Brain Sci 2022;12(5):562; doi: 10.3390/brainsci12050562

37. Pio-Lopez L, Levin M. Morphoceuticals: Perspectives for discovery of drugs targeting anatomical control mechanisms in regenerative medicine, cancer and aging. Drug Discov Today 2023;28(6):103585; doi: 10.1016/j.drudis.2023.103585

38. Tabibzadeh S, Brown OR. Trending toward gero-electroceuticals that target membrane potential for reprogramming aging and lifespan. Aging and Cancer 2024;5(1–2):3–13; doi: 10.1002/aac2.12070

39. Sundelacruz S, Levin M, Kaplan DL. Membrane potential controls adipogenic and osteogenic differentiation of mesenchymal stem cells. PLoS One 2008;3(11):e3737; doi: 10.1371/journal.pone.0003737

40. Huang Y, Yao K, Zhang Q, et al. Bioelectronics for electrical stimulation: Materials, devices and biomedical applications. Chem Soc Rev 2024;53(17):8632–8712; doi: 10.1039/d4cs00413b

41. Vogg MC, Buzgariu W, Suknovic NS, et al. Cellular, metabolic, and developmental dimensions of whole-body regeneration in hydra. Cold Spring Harb Perspect Biol 2021;13(12):a040725; doi: 10.1101/cshperspect.a040725

42. Tomczyk S, Fischer K, Austad S, et al. Hydra, a powerful model for aging studies. Invertebr Reprod Dev 2015;59(sup1):11–16; doi: 10.1080/07924259.2014.927805

43. Reiter S, Crescenzi M, Galliot B, et al. Hydra, a versatile model to study the homeostatic and developmental functions of cell death. Int J Dev Biol 2012;56(6–8):593–604; doi: 10.1387/ijdb.123499sr

44. Lenhoff HM, Loomis WF. The Biology of Hydra and of Some Other Coelenterates, 1961. University of Miami Press: Miami, FL; 1961.

45. Galliot B. Hydra, a fruitful model system for 270 years. Int J Dev Biol 2012;56(6–8):411–423; doi: 10.1387/ijdb.120086bg

46. Böttger A, Hassel M. Hydra, a model system to trace the emergence of boundaries in developing eumetazoans. Int J Dev Biol 2012;56(6–8):583–591; doi: 10.1387/ijdb.113454ab

47. Bode HR. Axial patterning in hydra. Cold Spring Harb Perspect Biol 2009;1(1):a000463; doi: 10.1101/cshperspect.a000463

48. Rachamim T, Sher D. What Hydra can teach us about chemical ecology—How a simple, soft organism survives in a hostile aqueous environment. Int J Dev Biol 2012;56(6–8):605–611; doi: 10.1387/ijdb.113474tr

49. Quinn B, Gagné F, Blaise C. Hydra, a model system for environmental studies. Int J Dev Biol 2012;56(6–8):613–625; doi: 10.1387/ijdb.113469bq

50. Augustin R, Fraune S, Bosch TC. How Hydra senses and destroys microbes. Semin Immunol 2010;22(1):54–58; doi: 10.1016/j.smim.2009.11.002

51. Bode HR. Head regeneration in Hydra. Dev Dyn 2003; 226(2):225–236; doi: 10.1002/dvdy.10225

52. Bosch TC. Why polyps regenerate and we don't: Towards a cellular and molecular framework for Hydra regeneration. Dev Biol 2007;303(2):421–433; doi: 10.1016/j.ydbio .2006.12.012

53. Braun E, Keren K. Hydra regeneration: Closing the loop with mechanical processes in morphogenesis. Bioessays 2018;40(7):e1700204; doi: 10.1002/bies.201700204

54. Deines P, Lachnit T, Bosch TCG. Competing forces maintain the Hydra metaorganism. Immunol Rev 2017;279(1): 123–136; doi: 10.1111/imr.12564

55. Newman SA. The interaction of the organizing regions in hydra and its possible relation to the role of the cut end in regeneration. J Embryol Exp Morphol 1974;31(3):541–555; doi: 10.1242/dev.31.3.541

56. Newman SA. Reversible abolition of normal morphology in Hydra. Nat New Biol 1973;244(134):126–128; doi: 10 .1038/newbio244126a0

57. Domazet-Lošo T, Klimovich A, Anokhin B, et al. Naturally occurring tumours in the basal metazoan Hydra. Nat Commun 2014;5:4222; doi: 10.1038/ncomms5222

58. Boutry J, Mistral J, Berlioz L, et al. Tumors (re)shape biotic interactions within ecosystems: Experimental evidence from the freshwater cnidarian Hydra. Sci Total Environ 2022;803:149923; doi: 10.1016/j.scitotenv.2021.149923

59. Boutry J, Buysse M, Tissot S, et al. Spontaneously occurring tumors in different wild-derived strains of hydra. Sci Rep 2023;13(1):7449; doi: 10.1038/s41598-023-34656-0

60. Yuste R. Breaking the neural code of a cnidarian: Learning principles of neuroscience from the "vulgar" Hydra. Curr Opin Neurobiol 2024;86:102869; doi: 10.1016/j.conb.2024 .102869

61. Szymanski JR, Yuste R. Mapping the whole-body muscle activity of *Hydra vulgaris*. Curr Biol 2019;29(11): 1807–1817. e1803; doi: 10.1016/j.cub.2019.05.012

62. Dupre C, Yuste R. Non-overlapping neural networks in *Hydra vulgaris*. Curr Biol 2017;27(8):1085–1097; doi: 10 .1016/j.cub.2017.02.049

63. Hanson A. Spontaneous electrical low-frequency oscillations: A possible role in Hydra and all living systems. Philos Trans R Soc Lond B Biol Sci 2021;376(1820): 20190763; doi: 10.1098/rstb.2019.0763

64. David CN, Schmidt N, Schade M, et al. Hydra and the evolution of apoptosis. Integr Comp Biol 2005;45(4):631–638; doi: 10.1093/icb/45.4.631

65. Schenkelaars Q, Tomczyk S, Wenger Y, et al. Model system for deciphering the mechanisms of aging and resistance to aging. In: Conn's Handbook of Models for Human Aging. Ram JL and Conn PM, eds. Academic Press: Cambridge, MA; 2018; pp. 507–520.

66. Adams DS, Levin M. Measuring resting membrane potential using the fluorescent voltage reporters DiBAC4(3) and CC2-DMPE. Cold Spring Harb Protoc 2012;2012(4): 459–464; doi: 10.1101/pdb.prot067702

67. Adams DS, Levin M. General principles for measuring resting membrane potential and ion concentration using fluorescent bioelectricity reporters. Cold Spring Harb Protoc 2012;2012(4):385–397; doi: 10.1101/pdb.top067710

68. McMillen P, Levin M. Optical estimation of bioelectric patterns in living embryos. Methods Mol Biol 2024;2745: 91–102; doi: 10.1007/978-1-0716-3577-3_6

69. Martínez DE, Bridge D. Hydra, the everlasting embryo, confronts aging. Int J Dev Biol 2012;56(6–8):479–487; doi: 10.1387/ijdb.113461dm

70. Brien P. La pérennité somatique. Biol Rev Camb Philos Soc 1953;28(3):308–349; doi: 10.1111/j.1469-185x.1953 .tb01381.x

71. Yoshida K, Fujisawa T, Hwang JS, et al. Degeneration after sexual differentiation in hydra and its relevance to the evolution of aging. Gene 2006;385:64–70; doi: 10.1016/j .gene.2006.06.031

72. Pai VP, Lemire JM, Paré JF, et al. Endogenous gradients of resting potential instructively pattern embryonic neural tissue via Notch signaling and regulation of proliferation. J Neurosci 2015;35(10):4366–4385; doi: 10.1523/JNEUROSCI.1877-14 .2015

73. van Munster EB, Gadella TW. Fluorescence lifetime imaging microscopy (FLIM). Adv Biochem Eng Biotechnol 2005;95:143–175; doi: 10.1007/b102213

74. Python Software Foundation. (n.d.). IDLE.

75. Miller EW, Lin JY, Frady EP, et al. Optically monitoring voltage in neurons by photo-induced electron transfer through molecular wires. Proc Natl Acad Sci U S A 2012; 109(6):2114–2119; doi: 10.1073/pnas.1120694109

76. Team RC. R: A language and environment for statistical computing. R Foundation for Statistical Computing 2020.

77. Shapiro SS, Wilk MB. An analysis of variance test for normality (Complete Samples). Biometrika 1965;52(3–4): 591–611; doi: 10.2307/2333709

78. Kruskal WH, Wallis WA. Use of ranks in one-criterion variance analysis. J Am Stat Assoc 1952;47(260):583–621; doi: 10.1080/01621459.1952.10483441

79. Gibbons JD, Chakraborti S. Nonparametric Statistical Inference. Taylor & Francis Ltd: Boca Raton, FL; 2010; 9781439896129.

80. Hollander M, Wolfe DA, Chicken E. Nonparametric Statistical Methods. John Wiley & Sons Inc: Hoboken, NJ; 2014.

81. Hirvonen LM, Suhling K. Fast timing techniques in FLIM applications. Front Phys 2020;8; doi: 10.3389/fphy.2020 .00161

82. Tomczyk S, Buzgariu W, Perruchoud C, et al. Loss of neurogenesis in aging Hydra. Dev Neurobiol 2019;79(5): 479–496; doi: 10.1002/dneu.22676

83. Boggess SC, Lazzari-Dean JR, Raliski BK, et al. Fluorescence lifetime predicts performance of voltage sensitive fluorophores in cardiomyocytes and neurons. RSC Chem Biol 2021;2(1):248–258; doi: 10.1039/d0cb00152j

84. Deal PE, Grenier V, Kulkarni RU, et al. Making life visible: Fluorescent indicators to probe membrane potential. In: Make life visible. Springer: Singapore; 2020; pp. 89–104.

85. Lazzari-Dean JR, Gest AM, Miller EW. Optical estimation of absolute membrane potential using fluorescence lifetime imaging. Elife 2019;8:e44522; doi: 10.7554/eLife.44522

86. Efimov IR, Nikolski VP, Salama G. Optical imaging of the heart. Circ Res 2004;95(1):21–33; doi: 10.1161/01.RES .0000130529.18016.35

87. O'Shea C, Winter J, Kabir SN, et al. High resolution optical mapping of cardiac electrophysiology in pre-clinical

models. Sci Data 2022;9(1):135; doi: 10.1038/s41597-022-01253-1

88. Prindle A, Liu J, Asally M, et al. Ion channels enable electrical communication in bacterial communities. Nature 2015;527(7576):59–63; doi: 10.1038/nature15709

89. Fromm J, Lautner S. Electrical signals and their physiological significance in plants. Plant Cell Environ 2007;30(3):249–257; doi: 10.1111/j.1365-3040.2006.01614.x

90. Zhao DJ, Chen Y, Wang ZY, et al. High-resolution non-contact measurement of the electrical activity of plants in situ using optical recording. Sci Rep 2015;5:13425; doi: 10.1038/srep13425

91. Grinvald A, Anglister L, Freeman JA, et al. Real-time optical imaging of naturally evoked electrical activity in intact frog brain. Nature 1984;308(5962):848–850; doi: 10.1038/308848a0

92. Orbach HS, Cohen LB. Optical monitoring of activity from many areas of the in vitro and in vivo salamander olfactory bulb: A new method for studying functional organization in the vertebrate central nervous system. J Neurosci 1983;3(11):2251–2262; doi: 10.1523/JNEUROSCI.03-11-02251.1983

93. Kauer JS, Senseman DM, Cohen LB. Odor-elicited activity monitored simultaneously from 124 regions of the salamander olfactory bulb using a voltage-sensitive dye. Brain Res 1987;418(2):255–261; doi: 10.1016/0006-8993(87)90093-x

94. Friedrich RW, Korsching SI. Combinatorial and chemotopic odorant coding in the zebrafish olfactory bulb visualized by optical imaging. Neuron 1997;18(5):737–752; doi: 10.1016/s0896-6273(00)80314-1

95. Friedrich RW, Korsching SI. Chemotopic, combinatorial, and noncombinatorial odorant representations in the olfactory bulb revealed using a voltage-sensitive axon tracer. J Neurosci 1998;18(23):9977–9988; doi: 10.1523/JNEUROSCI.18-23-09977.1998

96. Wachowiak M, Cohen LB, Zochowski MR. Distributed and concentration-invariant spatial representations of odorants by receptor neuron input to the turtle olfactory bulb. J Neurophysiol 2002;87(2):1035–1045; doi: 10.1152/jn.00522.2001

97. Kamino K, Komuro H, Sakai T, et al. Functional pacemaking area in the early embryonic chick heart assessed by simultaneous multiple-site optical recording of spontaneous action potentials. J Gen Physiol 1988;91(4):573–591; doi: 10.1085/jgp.91.4.573

98. Lee P, Quintanilla JG, Alfonso-Almazán JM, et al. In vivo ratiometric optical mapping enables high-resolution cardiac electrophysiology in pig models. Cardiovasc Res 2019;115(11):1659–1671; doi: 10.1093/cvr/cvz039

99. Rentschler S, Vaidya DM, Tamaddon H, et al. Visualization and functional characterization of the developing murine cardiac conduction system. Development 2001;128(10):1785–1792; doi: 10.1242/dev.128.10.1785

100. Tang Q, Tsytsarev V, Frank A, et al. In vivo mesoscopic voltage-sensitive dye imaging of brain activation. Sci Rep 2016;6:25269; doi: 10.1038/srep25269

101. Osephson RK, Macklin M. Electrical properties of the body wall of Hydra. J Gen Physiol 1969;53(5):638–665; doi: 10.1085/jgp.53.5.638

102. Levin M, Pezzulo G, Finkelstein JM. Endogenous bioelectric signaling networks: Exploiting voltage gradients for control of growth and form. Annu Rev Biomed Eng 2017;19:353–387; doi: 10.1146/annurev-bioeng-071114-040647

103. Adams DS, Robinson KR, Fukumoto T, et al. Early, H+-V-ATPase-dependent proton flux is necessary for consistent left-right patterning of non-mammalian vertebrates. Development 2006;133(9):1657–1671; doi: 10.1242/dev.02341

104. Levin M, Thorlin T, Robinson KR, et al. Asymmetries in H+/K+-ATPase and cell membrane potentials comprise a very early step in left-right patterning. Cell 2002;111(1):77–89; doi: 10.1016/s0092-8674(02)00939-x

105. Beane WS, Morokuma J, Adams DS, et al. A chemical genetics approach reveals H, K-ATPase-mediated membrane voltage is required for planarian head regeneration. Chem Biol 2011;18(1):77–89; doi: 10.1016/j.chembiol.2010.11.012

106. Pezzulo G, LaPalme J, Durant F, et al. Bistability of somatic pattern memories: Stochastic outcomes in bioelectric circuits underlying regeneration. Philos Trans R Soc Lond B Biol Sci 2021;376(1821):20190765; doi: 10.1098/rstb.2019.0765

107. Rodrigues M, Leclère P, Flammang P, et al. The cellular basis of bioadhesion of the freshwater polyp Hydra. BMC Zool 2016;1(1):1–15; doi: 10.1186/s40850-016-0005-7

108. Gitter AH, Oliver D, Thurm U. Calcium- and voltage-dependence of nematocyst discharge in *Hydra vulgaris*. J Comp Physiol A 1994;175(1):115–122; doi: 10.1007/bf00217442

109. Nin V, Hernández JA, Chifflet S. Hyperpolarization of the plasma membrane potential provokes reorganization of the actin cytoskeleton and increases the stability of adherens junctions in bovine corneal endothelial cells in culture. Cell Motil Cytoskeleton 2009;66(12):1087–1099; doi: 10.1002/cm.20416

110. Smithers HE, Terry JR, Brown JT, et al. Aging-associated changes to intrinsic neuronal excitability in the bed nucleus of the stria terminalis is cell type-dependent. Front Aging Neurosci 2017;9:424; doi: 10.3389/fnagi.2017.00424

111. Thibault O, Hadley R, Landfield PW. Elevated postsynaptic [Ca2+]i and L-type calcium channel activity in aged hippocampal neurons: Relationship to impaired synaptic plasticity. J Neurosci 2001;21(24):9744–9756; doi: 10.1523/JNEUROSCI.21-24-09744.2001

112. Chang YM, Rosene DL, Killiany RJ, et al. Increased action potential firing rates of layer 2/3 pyramidal cells in the prefrontal cortex are significantly related to cognitive performance in aged monkeys. Cereb Cortex 2005;15(4):409–418; doi: 10.1093/cercor/bhh144

113. Hardy CC, Al-Naggar IM, Kuo CL, et al. Aging changes in bladder hyperpolarization-activated cyclic nucleotide-gated channels are associated with increasing heterogeneity of adrenergic/mucosal influence on detrusor control in the mouse. J Gerontol A Biol Sci Med Sci 2021;76(7):1153–1160; doi: 10.1093/gerona/glab070

114. Baker EC, Layden MJ, van Rossum DB, et al. Functional characterization of cnidarian HCN channels points to an early evolution of Ih. PLoS One 2015;10(11):e0142730; doi: 10.1371/journal.pone.0142730

115. Levin M, Martyniuk CJ. The bioelectric code: An ancient computational medium for dynamic control of growth and form. Biosystems 2018;164:76–93; doi: 10.1016/j.biosystems.2017.08.009

116. Pai VP, Lemire JM, Chen Y, et al. Local and long-range endogenous resting potential gradients antagonistically

regulate apoptosis and proliferation in the embryonic CNS. Int J Dev Biol 2015;59(7–9):327–340; doi: 10.1387/ijdb .150197ml

117. Pai VP, Levin M. HCN2 channel-induced rescue of brain, eye, heart and gut teratogenesis caused by nicotine, ethanol and aberrant notch signalling. Wound Repair Regen 2022; 30(6):681–706; doi: 10.1111/wrr.13032

118. Pai VP, Cervera J, Mafé S, et al. HCN2 channel-induced rescue of brain teratogenesis via local and long-range bio-electric repair. Front Cell Neurosci 2020;14:136; doi: 10 .3389/fncel.2020.00136

119. Pai VP, Pietak A, Willocq V, et al. HCN2 rescues brain defects by enforcing endogenous voltage pre-patterns. Nat Commun 2018;9(1):998; doi: 10.1038/s41467-018-03334-5

120. Juliano CE, Lin H, Steele RE. Generation of transgenic Hydra by embryo microinjection. J Vis Exp 2014(91): 51888; doi: 10.3791/51888

121. Anton-Erxleben F, Thomas A, Wittlieb J, et al. Plasticity of epithelial cell shape in response to upstream signals: A whole-organism study using transgenic Hydra. Zoology (Jena) 2009;112(3):185–194; doi: 10.1016/j.zool.2008.09 .002

122. Khalturin K, Anton-Erxleben F, Milde S, et al. Trans-genic stem cells in Hydra reveal an early evolutionary origin for key elements controlling self-renewal and differentiation. Dev Biol 2007;309(1):32–44; doi: 10 .1016/j.ydbio.2007.06.013

123. Wittlieb J, Khalturin K, Lohmann JU, et al. Transgenic Hydra allow in vivo tracking of individual stem cells dur-ing morphogenesis. Proc Natl Acad Sci U S A 2006; 103(16):6208–6211; doi: 10.1073/pnas.0510163103

124. Braun E, Ori H. Electric-induced reversal of morphogene-sis in Hydra. Biophys J 2019;117(8):1514–1523; doi: 10 .1016/j.bpj.2019.09.007

125. Agam O, Braun E. Stochastic morphological swings in *Hydra* regeneration: A manifestation of noisy canalized morphogenesis. Proc Natl Acad Sci U S A 2025;122(1): e2415736121; doi: 10.1073/pnas.2415736121

Address correspondence to:
Michael Levin, PhD
Department of Biology
Tufts University
200 Boston Avenue
Suite 4600, Medford
MA 02155
USA

E-mail: michael.levin@allencenter.tufts.edu